POLITECNICO DI TORINO
Repository ISTITUZIONALE

The contribution of largescale atmospheric circulation to variations of observed nearsurface wind speed across Sweden since 1926

Original
The contribution of largescale atmospheric circulation to variations of observed nearsurface wind speed across Sweden since 1926 / Minola, L., Lönn, J., Azorinmolina, C., Zhou, C., Engström, E., Wern, L., Hellström, S., Zhang, G., Shen, C., Pezzoli, A., Chen, D.. - In: CLIMATIC CHANGE. - ISSN 1573-1480. - ELETTRONICO. - 176:54(2023), pp. 1-22. [10.1007/s10584-023-03525-0]

Availability:
This version is available at: 11583/2978330 since: 2023-05-04T08:35:52Z

Publisher:
Springer

Published
DOI:10.1007/s10584-023-03525-0

Terms of use:

This article is made available under terms and conditions as specified in the corresponding bibliographic description in the repository

Publisher copyright

(Article begins on next page)

11 September 2026

Climatic Change (2023) 176:54
https://doi.org/10.1007/s10584-023-03525-0

The contribution of large-scale atmospheric circulation to variations of observed near-surface wind speed across Sweden since 1926

Lorenzo Minola[1,2,3] · Jessika Lönn[1] · Cesar Azorin-Molina[3] · Chunlüe Zhou[1] · Erik Engström[4] · Lennart Wern[4] · Sverker Hellström[4] · Gangfeng Zhang[5,6] · Cheng Shen[1] · Alessandro Pezzoli[2] · Deliang Chen[1]

Received: 10 November 2022 / Accepted: 26 March 2023
© The Author(s) 2023

Abstract
This study investigates the centennial-scale (i.e., since 1926) variability of observed near-surface wind speed across Sweden. Results show that wind speed underwent various phases of change during 1926–2019, i.e., (a) a clear slowdown during 1926–1960; (b) a stabilization from 1960 to 1990; (c) another clear slowdown during 1990–2003; (d) a slight recovery/stabilization period for 2003–2014, which may continue with a possible new slowdown. Furthermore, the performance of three reanalysis products in representing past wind variations is evaluated. The observed low-frequency variability is properly simulated by the selected reanalyses and is linked to the variations of different large-scale atmospheric circulation patterns (e.g., the North Atlantic Oscillation). However, the evident periods of decreasing trend during 1926–1960 and 1990–2003, which drive most of the stilling in the last century, are missing in the reanalyses and cannot be realistically modeled through multiple linear regression by only using indexes of atmospheric circulation. Therefore, this study reveals that changes in large-scale atmospheric circulation mainly drive the low-frequency variability of observed near-surface wind speed, while other factors (e.g., changes in surface roughness) are crucial for explaining the periods of strong terrestrial stilling across Sweden.

Keywords Wind speed · Climate variability · Centennial-scale · Twentieth century reanalysis · Large-scale atmospheric circulation · Sweden

1 Introduction

Near-surface wind speed (hereafter, NSWS) is a key factor in transferring heat, moisture, energy, and momentum between the Earth's surface and the atmosphere (Abhishek et al. 2010). By controlling the evaporation demand, surface winds can alter the hydrological cycle and partly affect agriculture productivity (Rayner 2007; McVicar et al. 2012). NSWS

✉ Lorenzo Minola
lorenzo.minola@gu.se

Extended author information available on the last page of the article

regulates as well the accumulation and dispersion of air pollutants near emission sources, such as traffic in urban areas (Grundström et al. 2015); it can also contribute to the cooling in urban heat islands (Bing et al. 2021), and it strongly impacts soil erosion over many dry land regions (Zhang et al. 2019). In addition, as the development of renewable energy resources is central to energy scenarios that help keeping warming below 2 °C (IPCC 2014), society relies on electricity production from wind farms when it comes to the reduction of greenhouse gas emissions (Zeng et al. 2019). For example, in Sweden, wind power stood for about 16% of the overall energy production in 2020 (Berard 2021).

For all the mentioned reasons, it is crucial to understand how NSWS has been and will be affected by a warmer climate, so that society can adapt to the expected new wind scenarios (IPCC 2013). Therefore, over the last few decades, various studies have investigated multidecadal changes in observed NSWS across various areas of the globe (e.g., Azorin-Molina et al. 2014; Laapas and Venäläinen 2017). It has been reported a general slowdown in NSWS over land in most northern midlatitude regions during the last 30–50 years (McVicar et al. 2012). Such a general slowdown in terrestrial winds, which has been named "stilling" by Roderick et al. (2007), differs from the opposite increase in NSWS revealed over large parts of the oceans (Zheng et al. 2016). However, recent studies have also evidenced a recovery in the observed terrestrial NSWS decline during the last decades (Kim and Paik 2015; Zhang and Wang 2020). Such a break in the terrestrial stilling became prominent since around 2010 across the Northern Hemisphere, especially in Europe, North America, and East Asia (Zeng et al. 2019).

Even if the exact reasons behind the terrestrial stilling and its reversal are unclear, different possible causes have been proposed. Vautard et al. (2010) showed that the increase in surface roughness (e.g., urbanization, land-use changes, forest growth) may be the main reason behind the terrestrial decrease in NSWS. But this differs from what was found by Zeng et al. (2018), who argued that the increase in vegetation cover has had only a limited influence on the wind stilling. Large-scale atmospheric circulation has been identified by many studies as a key driver for NSWS variations and changes (Wu et al. 2018). In fact, in a changing climate, regional warming differences control variations of regional surface pressure gradients, which modulate circulation patterns (Lin et al. 2013). For instance, phase changes of the North Atlantic Oscillation (Azorin-Molina et al. 2018a; Minola et al. 2021) and of the Pacific Decadal Oscillation (Zeng et al. 2019) have been linked to the reversal in the terrestrial stilling. The aging of measuring instruments has also been suggested as a potential cause of the NSWS decrease (Azorin-Molina et al. 2018b).

Previous studies have already investigated NSWS changes and variations across Sweden. In particular, Minola et al. (2016) looked at the multidecadal variability in observed NSWS during 1956–2013. An overall statistically significant slowdown was found, but strong differences in the seasonal trends were also found (i.e., weak increase in winter and strong stilling in spring, summer, and autumn). Such seasonal differences could be explained by the impact of large-scale atmospheric circulation, in particular by the influence of the North Atlantic Oscillation, especially when it comes to modulate winter NSWS variability. In addition, Minola et al. (2021) investigated NSWS changes across Sweden for the recent past two decades (i.e., 1997–2019), which were only partly covered by Minola et al. (2016). Here it is shown that the stilling ceased in 2003, and no clear trend can be detected afterwards. Such stilling-reversal pattern was linked to changes in the North Atlantic Oscillation. Furthermore, this study revealed that changes in surface roughness (e.g., changes in forest cover) contributed to the general slowdown detected for 1997–2019.

As NSWS varies on multiple temporal scales, sufficiently long data series are necessary for a meaningful assessment of climate variability (IPCC 2021). Even though climate

journals may store valuable old not-digitized climate data (Engström et al. 2022), studies on NSWS changes have only focused over the last ~60 years as reliable, continuous, and easy-to-access observations lack over a longer time window. Because NSWS observations are almost absent at the centennial scale, alternative datasets, such as twentieth century reanalyses (i.e., developed to cover the entire twentieth century), have been largely used to investigate the centennial-scale variability in NSWS (Bett et al. 2017; Shen et al. 2021a). In fact, by using a forecast model in which information from observations are assimilated (Dee et al. 2011), reanalyses provide spatially complete and physically coherent simulated data. However, any climate-variability result obtained by using reanalysis products must be evaluated against in situ measurements data as the reanalysis performance is strongly dependent on the considered time period and the selected study area (Ramon et al. 2019; Yu et al. 2019).

For all the mentioned reasons, this study aims at investigating centennial-scale (since 1926) variations and changes in observed NSWS across Sweden. No other dataset of observed NSWS has been investigated before for such a long time period. By comparing observed series against the ones from reanalysis products, the performance of current climate reanalyses in reproducing past changes in NSWS across Sweden on a centennial time scale is also evaluated. In addition, the impact of large-scale atmospheric circulation on the detected variations is explored by quantifying its contribution to the NSWS variability.

2 Data

2.1 NSWS observations

NSWS observations across Sweden are available for downloading at: https://www.smhi.se/data/utforskaren-oppna-data/ (last accessed 9 March 2023). At this link, it is possible to access only wind data which has been measured, digitized, and later stored at the archive servers of the Swedish Meteorological and Hydrological Institute (SMHI). Reliable and continuous NSWS measurements that can be downloaded here start only in the 1950s at the earliest (Minola et al. 2016). But there are still valuable wind observations that have not been digitized yet, which are stored on paper climate journals at the SMHI archive in Norrköping. Therefore, to create the longest-available century-long NSWS dataset, through the work of Engström et al. (2022), wind measurements were rescued and digitized by scanning old weather journals from 1920 to 1940. The resulting dataset is constituted by rescued NSWS series from 13 measuring stations, which contain observations since the early 20s. To remove any non-climatic change point, a four-step homogenization procedure was later applied to the monthly mean observed NSWS series. More details about how the observed series were homogenized can be found in Zhou et al. (2022). However, the rescued and homogenized 13 stations do not all cover the same time period (e.g., only two stations are still active today, most stations have observations until the 90s) and contain large periods of missing values. Therefore, we select only 7 stations that cover NSWS observations for the 71-year 1926–1996 period with a maximum of 5% of missing data (i.e., 42 months). The 1926–1996 time window was selected as it was identified as the time period that most of the stations can cover with not too many missing values. Figure 1 shows the location of the 7 stations selected in the NSWS dataset which will be analyzed here. Unfortunately, all the stations from the west coast of Sweden were discarded (as they contain long periods of missing data).

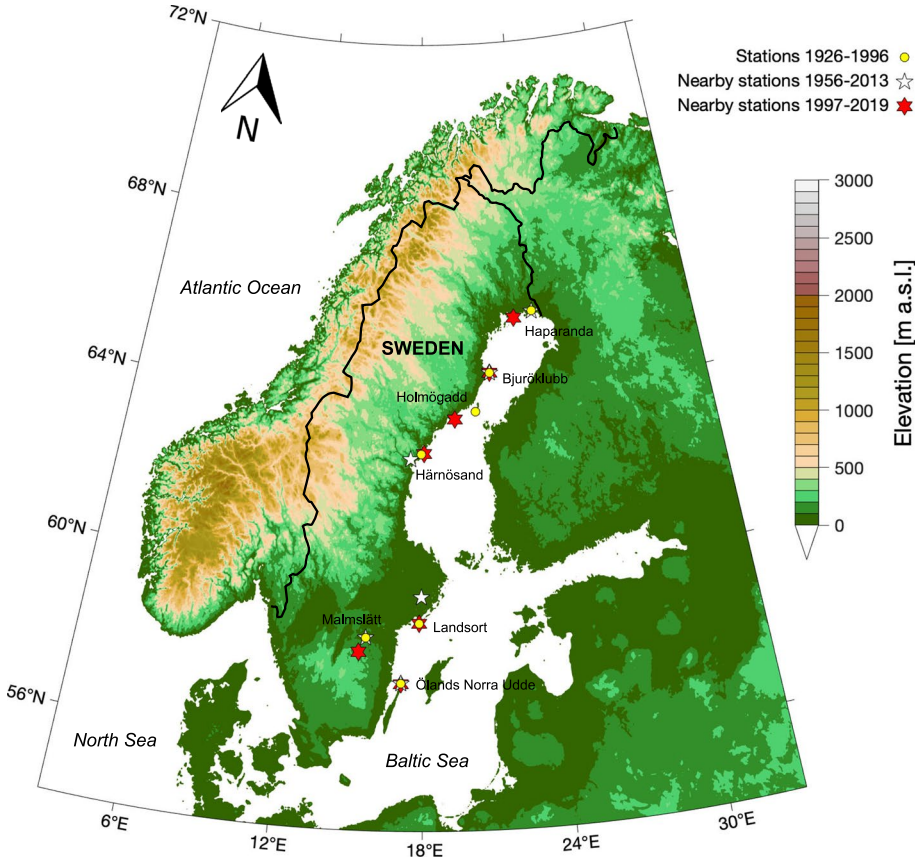

Fig. 1 Map of the location of the measuring stations selected for the 1926–1996 dataset (yellow dots) together with the location of the nearby stations from Minola et al. (2016) (1956–2013 dataset; white stars) and Minola et al. (2021) (1997–2019 dataset; red hexagons)

Since the rescued NSWS dataset covers only 1926–1996, in order to investigate NSWS changes also after 1997, we complement this dataset with NSWS measurements from two previous studies: (i) homogenized NSWS observations for 1956–2013 from Minola et al. (2016); and (ii) homogenized NSWS observations for 1997–2019 from Minola et al. (2021). By comparing those three datasets, we can thus investigate changes and variations in NSWS across Sweden during 1926–2019, i.e., over almost a century. To make an accurate comparison, from the datasets of Minola et al. (2016) and Minola et al. (2021) we only select the same stations from the 1926–1996 dataset. If the same station does not appear in those two datasets, we select the nearest station available (see Fig. 1). For Holmögadd station, the nearest station in the 1956–2013 dataset is Bjuröklubb (at 106 km distance), which is already included as the nearby station. Therefore, for the dataset 1956–2013, only 6 stations are used for representing the regional mean.

2.2 NSWS from reanalyses

This study compares observed NSWS with wind outputs of three different reanalyses: (a) the European Center for Medium-Range Weather Forecasts (ECMWF) twentieth century reanalysis (hereafter, ERA20C); (b) the fifth generation ECMWF reanalysis (hereafter, ERA5); and (c) the National Oceanic and Atmospheric Administration–Cooperative Institute for Research in Environmental Sciences (NOAA-CIRES) twentieth century reanalysis, version 2c (hereafter, 20CR). ERA20C is the ECMWF's first atmospheric reanalysis of the twentieth century, covering the 1900–2010 time period (Poli et al. 2016). By assimilating only observations of surface pressure and surface marine winds, it models various climatic variables at a horizontal resolution of ~125 km, with a 3-hourly temporal resolution. Instead, ERA5 is the latest modern reanalysis product of ECMWF (Hersbach et al. 2020). It delivers hourly outputs at a horizontal grid spacing of ~31 km from 1950 to the present. Contrary to ERA20C, which assimilates only surface pressure and surface marine wind observations, ERA5 combines a large amount of different historical observations using advanced modeling and data assimilation systems. It also assimilates terrestrial vertical wind profiles from satellites, and radio- and aircraft-sondes, but it does not include NSWS observations over land as they cannot be fully interpreted by the data assimilation system (Dee et al. 2011). 20CR is a global gridded reanalysis produced by the collaboration between NOAA's Physical Sciences Laboratory and CIRES at the University of Colorado (Compo et al. 2011). It assimilates only surface observations of synoptic pressure into the NOAA's Global Forecast System and prescribes sea surface temperature and sea ice distribution for estimating various climate variables since 1836 on a $2.0° \times 2.0°$ latitude–longitude grid.

3-hourly wind data (i.e., u- and v-component) of ERA20C during 1900–2010 are downloaded from the ECMWF website (https://apps.ecmwf.int/datasets/data/era20c-daily/levtype=sfc/type=an/, last accessed 9 March 2023), while hourly wind outputs of ERA5 for 1950–2019 are accessed from the Copernicus website (https://cds.climate.copernicus.eu/cdsapp#!/dataset/reanalysis-era5-single-levels-preliminary-back-extension?tab=form and https://cds.climate.copernicus.eu/cdsapp#!/dataset/reanalysis-era5-single-levels?tab=form, last accessed 9 March 2023). Ensemble mean fields of 6-hourly wind components of 20RC are downloaded for 1900–2014 from https://downloads.psl.noaa.gov/Datasets/20thC_ReanV2c/gaussian/monolevel/, last accessed 9 March 2023). By using the u- (longitudinal) and v- (meridional) component of wind, the total wind speed is calculated at each time step using $\text{NSWS} = \sqrt{u^2 + v^2}$, and those outputs are then used to calculate the monthly mean series. Following Minola et al. (2020), each observed NSWS series is compared with the ERA20C and ERA5 wind series of the closest grid point to the measuring station, giving the assumption that the closest grid point simulates the observed wind better than any other more distant grid point.

2.3 Indexes of atmospheric circulation patterns

To explore the possible influence of large-scale atmospheric circulation on the NSWS variability across Sweden, the relationship between wind series and different atmospheric circulation modes is analyzed. In particular, here we look at these 4 climate indexes: (1) the North Atlantic Oscillation (hereafter, NAO) index; (2) the Arctic Oscillation (hereafter, AO) index; (3) the Scandinavian Pattern (hereafter, SCA) index; and (4) the East Atlantic

Pattern (hereafter, EA) index. NAO drives the shift of the Atlantic storm tracks across Europe, thus affecting how stormy the weather conditions are in Northern or Southern Europe (Hurrel et al. 2003). The NAO series for this study is obtained from https://crudata.uea.ac.uk/cru/data/nao/ (last accessed 9 March 2023). AO affects the north-to-south location of the storm-steering mid-latitude jet stream (Scott 2021). The centennial-scale AO series (i.e., until 2002) is downloaded from https://www.atmos.colostate.edu/~davet/ao/Data/ao_index.html (last accessed 9 March 2023). To be able to cover the more recent years (i.e., from 2002 to the present), AO index for 1950–2019 was obtained from https://www.cpc.ncep.noaa.gov/products/precip/CWlink/daily_ao_index/ao.shtml (last accessed 9 March 2023). The SCA pattern influences the exit region of the Atlantic jet stream from its climatological mean position, thus determining the preferred region of cyclone growth (Blackburn and Hoskins 2001). EA may play a role in positioning the North Atlantic storm track by modulating the location and strength of the NAO dipole (Moore et al. 2011). Centennial-scale SCA and EA series are retrieved from Comas-Bru and Hernández (2018) (https://doi.pangaea.de/10.1594/PANGAEA.892768?format=html#download, last accessed 9 March 2023).

3 Methods

3.1 Trend analyses

Trends in NSWS are represented by the slope of the applied regression analysis (i.e., linear regression) and are expressed as changes per decade (i.e., dec^{-1}). The magnitude of the linear trends is calculated using the non-parametric Sen's method (Gilbert 1987). Their significance is defined using the modified Mann–Kendall test (for considering the effect of statistically significant autocorrelation; Hamed and Ramachandra Rao 1998) and is reported at three different levels of significance: (1) significant at $p < 0.05$; (2) significant at $p < 0.10$; and (3) non-significant at $p > 0.10$ (Azorin-Molina et al. 2014). On top of the linear trends, the Gaussian low-pass filter with a 15-year window is used to show the low-frequency variability of the time series. When possible, NSWS series are expressed as anomaly series: in this way, when calculating regional means, more windy series do not dominate the regional NSWS series (Azorin-Molina et al. 2014). For example, for the 1926–1996 dataset, anomalies are calculated as the deviation from 1926 to 1996. But when it comes to the comparison between the datasets 1926–1996, 1956–2013, and 1997–2019, NSWS series cannot be expressed as anomalies as there is no common time period for all the series. Analyses are carried out for annual and seasonal series.

3.2 Statistics of comparison

To mathematically evaluate the agreement between different series, the following statistical tests are used: (1) Pearson's correlation coefficient (hereafter, r), to measure the degree of association (i.e., linear relationship; Gibbons and Chakraborti 2003); (2) root mean squared error (hereafter, RMSE), to mathematically express the vicinity between two series (Von Storch and Zwiers 1999); and (3) bias, to identify the tendency to constant deviate of a realization compared to another.

3.3 Multiple linear regression

To quantify the contribution of large-scale atmospheric circulation to NSWS variability, variance based on multiple linear regression (hereafter, MLR) is used (Pedroni 1999; Shi et al. 2019). In particular, by using the indexes of teleconnection patterns (one or more of them) as independent variables and the NSWS as the true realization, regression coefficients are calculated based on multiple regression theory. Those regression coefficients, in combination with the circulation indexes, are then used to calculate the simulated NSWS, which expresses NSWS variability only driven by large-scale atmospheric circulation variations. The match/mismatch between raw and reconstructed NSWS series is quantified through the coefficient of determination R^2 (Von Storch and Zwiers 1999). Under the hypothesis that the two series are equal, R^2 quantifies the ability of the simulated NSWS series to explain the variation of the raw NSWS series. R^2 values closer to 1 indicate a higher level of association.

4 Results

4.1 NSWS variability since 1926

Figure 2 shows the variability of the mean (i.e., average over all stations) annual and seasonal NSWS anomaly series during 1926–1996, while Table 1 summarizes their trends. Annually, an overall negative trend of -0.11 m s^{-1} dec^{-1} (statistically significant at $p < 0.05$) has been found during 1926–1996, even though periods of different signs of change occurred. In particular, three phases of NSWS changes can be identified during 1926–1996 (see Table 1): (a) a clear slowdown of -0.20 m s^{-1} dec^{-1} ($p < 0.05$) during 1926–1960; (b) a stabilization from 1960 to 1990 ($+0.01$ m s^{-1} dec^{-1}, non-significant at $p < 0.05$); and (c) the possible start of a new slowdown since 1990. Seasonally, winter is the season that shows the highest interannual variability, while summer is the lowest one (Fig. 2). All seasons display an overall significant ($p < 0.05$) slowdown of ~ -0.11 m s^{-1} dec^{-1} during 1926–1996 (Table 1), which is caused by a distinct decrease for 1960–1970, followed by a period of stabilization/recovery until $\sim$ 1990. Such a decreasing trend is more evident for summer and autumn, while for winter and spring, even if a general slowdown appears, the NSWS series are also dominated by interannual variabilities and by cycles of changes. To notice that the great negative NSWS anomaly observed in winter of 1996 strongly affects the winter (and therefore also the annual) trend for 1990–1996, which appears to be strongly negative, but not significant at $p < 0.05$.

To better understand the NSWS variability over Sweden during the last century, the 1926–1996 series of this study are compared with the ones from Minola et al. (2016) and Minola et al. (2021), able to cover the more recent decades. Therefore, by adding the 1956–2013 and 1997–2019 datasets to the rescued dataset, we can investigate NSWS variability from 1926 until 2019. As shown in Fig. 3, the 1926–1996 and the 1956–2013 mean (i.e., averaged over all the stations in the dataset) series display a similar variability during the common period 1956–1996: r have high values both annually and seasonally (e.g., for annual series, r is 0.85, statistically significant at $p < 0.05$). The 1956–2013 and 1997–2019 mean NSWS series also show a high correlation for the common 1997–2013 time period (e.g., annual r of 0.72, statistically significant at $p < 0.05$).

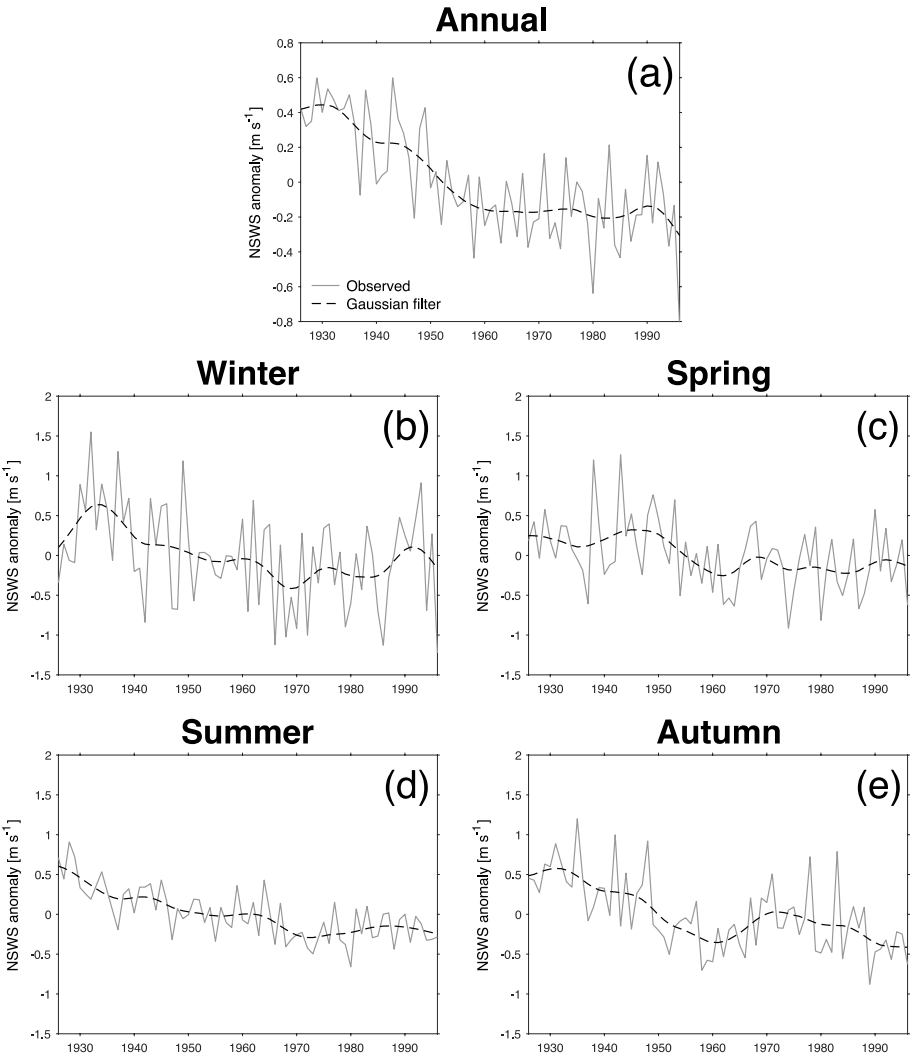

Fig. 2 Series of mean (i.e., average over all stations across Sweden) annual and seasonal NSWS anomalies for 1926–1996. Series are expressed as anomalies from the 1926–1996 mean. The low-frequency variability is shown with the black dashed lines of the applied Gaussian-weighted average (15-year windows)

Even though the three datasets correlate well with each other, they display differences in the magnitude of NSWS. Such biases may be related to the different homogenization techniques adopted and the different reference series used to detect breakpoints and adjust them. However, the high correlation values confirm that the series complement each other and can be used all together for investigating NSWS variabilities and changes during the extended period of 1926–2019. Annually, the stilling detected from 1990 continues until around 2003; it is then followed by a period of stabilization and weak recovery from such a strong decreasing trend. Those phases of change can be identified for all the seasons, even in winter and autumn under a stronger interannual variability

Table 1 Trends (m s^{-1} dec^{-1}) of the mean (i.e., average over all stations across Sweden) annual and seasonal NSWS anomalies for 1926–1996 and the sub-periods 1926–1960, 1960–2990, and 1990–1996. Statistically significant trends are shown in boldface for $p < 0.05$ and in italic for $p < 0.10$

Period	1926-1996	1926-1960	1960-1990	1990-1996
Annual	**-0.11**	**-0.20**	+0.01	**-1.19**
Winter	**-0.09**	-0.15	-0.01	-2.36
Spring	**-0.07**	*-0.10*	+0.01	-0.98
Summer	**-0.11**	**-0.18**	-0.02	-0.47
Autumn	**-0.12**	**-0.30**	+0.00	+0.25

compared to spring and summer. To summarize, five phases of NSWS changes can be identified during 1926–2019: (a) a clear slowdown during 1926–1960; (b) a stabilization from 1960 to 1990; (c) another clear slowdown during 1990–2003; (d) a slight recovery/stabilization period for 2003–2014; and (e) the possible start of a new slowdown since 2014 (difficult to evaluate as seen over only 5 years).

4.2 Comparison with variability in reanalysis products

Figure 4 compares the variability of simulated NSWS from ERA20C for 1900–2010 and 20CR for 1900–2014 against the variability of observed NSWS during 1926–1996, 1956–2013, and 1997–2019. Annually and seasonally, both the reanalyses do not capture the strong decrease observed during 1926–1960. Instead, for 1900–1990, they simulate a positive increase in NSWS (e.g., for annual series in ERA20C, 0.03 m s^{-1} dec^{-1} during 1900–1990, significant at $p < 0.05$). Similarly, also the evident stilling in observed NSWS for 1990–2013 does not have the same magnitude in the simulated trend of ERA20C and 20CR: in fact, from 1990 to 2010, the reanalyses also show a general decline, but such slowdown is not as evident and strong as the one in the observed dataset. Table 2 further explores the performance of the two reanalyses in representing observed NSWS by showing various statistics for comparison. While ERA20C tends to underestimate observed wind speed and 20CR overestimates NSWS, reanalyzed NSWS series well correlate with the observed series during winter, autumn, and summer (lower r values annually and during summer), even if they do not display the observed strong stilling during 1926–1960 and 1990–2003. Overall, although ERA20C and 20CR cannot reproduce the two stilling periods, they can represent well the overall interdecadal variability with its fluctuations in the change. For instance, the low-frequency variations of observed NSWS in spring during 1960–1990 are properly simulated by all the reanalyses.

Figure 4 also shows the variability of NSWS from ERA5 during 1950–2019 in comparison with the observed one for 1926–1996, 1956–2013, and 1997–2019, while Table 2 investigates the performance of this reanalysis in simulating observed NSWS variabilities. Like ERA20C and 20CR, this reanalysis cannot simulate the strong negative trend for 1926–1960 and 1990–2013. Instead, ERA5 well captures the weak variations occurring

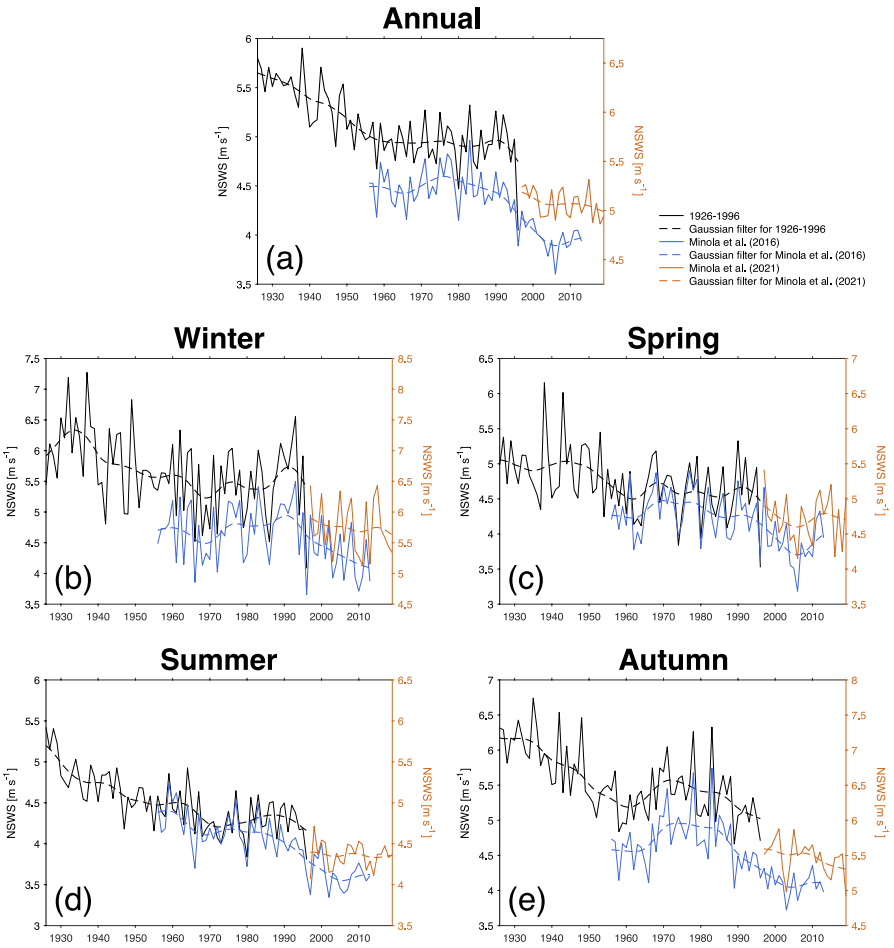

Fig. 3 Series of mean (i.e., average over all stations across Sweden) annual and seasonal NSWS for 1926–1996 (black line), 1956–2013 (from Minola et al. 2016; blue line), and 1997–2019 (from Minola et al. 2021; orange line). The low-frequency variability is shown with the dashed lines of the applied Gaussian-weighted average (15-year windows)

over the whole time period, such as the recovery after 2003 and the various cycles of changes during 1960–1990.

Overall, even if ERA20C, 20CR, and ERA5 differ in the observation data that they assimilate (see Sect. 2.2), all the reanalyses well agree in how they simulate the variations in NSWS over Sweden (Fig. 4 and Fig. S1 in the supplementary material). Annually and seasonally, correlation during the common time period 1950–2010 is always higher than 0.75 and significant at $p < 0.05$ (Table S1 in the supplementary material). As shown in Fig. 4, the reanalyses do not show the significant and strong decrease in NSWS as displayed by the observation dataset. Instead, they show periods of variations: those phases of change are similar in ERA20C, 20CR, and ERA5. Even if the correlation is high, ERA20C and ERA5 differ in a constant bias of ~0.6 m s^{-1}, ERA5 and 20CR in ~0.6 m s^{-1}, and ERA20C

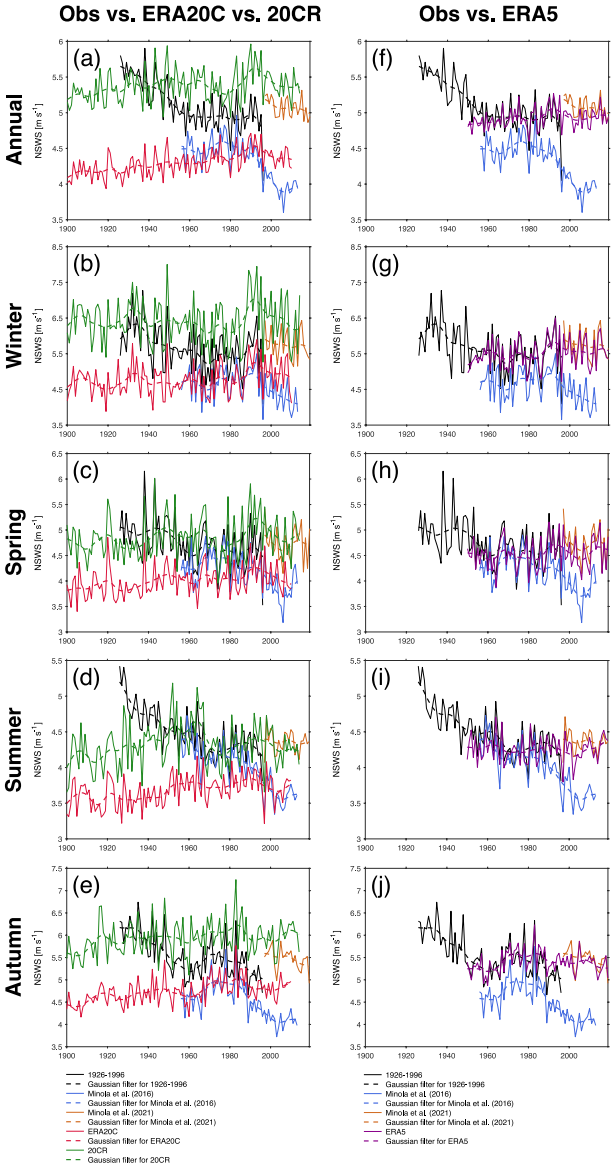

Fig. 4 Comparison between observed (black line for 1926–1996; blue line for 1956–2013 from Minola et al. 2016; orange line for 1997–2019 from Minola et al. 2021), ERA20C (red line, left column), 20CR (green line, left column), and ERA5 (violet line, right column) mean (i.e., average over all stations/nearby grid points) annual and seasonal NSWS series. The low-frequency variability is shown with the dashed lines of the applied Gaussian-weighted average (15-year windows).

and 20CR have a bias difference of ~1.0 m s^{-1} (Table S1 in the supplementary material). Overall, ERA20C simulates less strong wind compared to ERA5, while the modeled wind of 20CR is the strongest among the dataset here. From the comparison of Table 2, it is evident that ERA5 performs better than ERA20C and 20CR in simulating observed NSWS variability, most likely due to its higher resolution (which helps in the comparison between one grid point and single in-situ data), better model physics, more data assimilated, and its more advanced assimilation method (see Sect. 2.2).

Table 2 Annual and seasonal statistics for comparison between mean (i.e., average over all stations across Sweden) observed NSWS and reanalyzed NSWS from ERA20C for 1926–1996 (and 1956–2010), 20CR for 1926–1996 (and 1956–2013), and ERA5 for 1950–1996 (1956–2013). In particular, *r*, RMSE, and bias are shown. *r* coefficients statistically significant at $p < 0.05$ are shown in boldface

Obs *vs.* ERA20C for 1926-1996 (1956-2010)			
Period	***r***	**RMSE [m s^{-1}]**	**Bias [m s^{-1}]**
Annual	0.14 (0.34)	0.9 (0.3)	-0.8 (0.0)
Winter	**0.80** (**0.77**)	1.0 (0.4)	-0.9 (0.2)
Spring	**0.67** (**0.66**)	0.8 (0.3)	-0.7 (-0.1)
Summer	0.01 (**0.51**)	0.9 (0.4)	-0.9 (-0.3)
Autumn	**0.40** (**0.61**)	0.9 (0.4)	-0.8 (0.3)
Obs *vs.* 20CR for 1926-1996 (1956-2013)			
Period	***r***	**RMSE [m s^{-1}]**	**Bias [m s^{-1}]**
Annual	**0.37** (0.24)	0.5 (1.1)	0.3 (1.1)
Winter	**0.85** (**0.77**)	0.8 (1.9)	0.8 (1.8)
Spring	**0.67** (**0.52**)	0.4 (0.8)	0.1 (0.7)
Summer	**0.30** (**0.38**)	0.4 (0.5)	-0.1 (0.4)
Autumn	**0.51** (**0.52**)	0.6 (1.5)	0.4 (1.5)
Obs *vs.* ERA5 for 1950-1996 (1956-2013)			
Period	***r***	**RMSE [m s^{-1}]**	**Bias [m s^{-1}]**
Annual	**0.68 (0.36)**	0.2 (0.6)	0.0 (0.6)
Winter	**0.88 (0.80)**	0.3 (1.0)	0.0 (0.9)
Spring	**0.85 (0.67)**	0.2 (0.4)	-0.1 (0.3)
Summer	**0.74 (0.51)**	0.2 (0.4)	-0.1 (0.3)
Autumn	**0.80 (0.61)**	0.2 (1.0)	0.1 (0.9)

Table 3 Annual and seasonal Pearson's correlation coefficients between NSWS anomalies and the NAO index, the AO index, the SCA index, and the EA index for 1926–1996, 1956–2013, and 1997–2015. *r* coefficients statistically significant at $p < 0.05$ are shown in boldface

1926-1996				
Period	**NAO**	**AO**	**SCA**	**EA**
Annual	**+0.30**	**+0.31**	+0.01	+0.05
Winter	**+0.50**	**+0.53**	+0.03	**+0.31**
Spring	**+0.28**	**+0.53**	+0.08	**+0.45**
Summer	-0.04	-0.20	**-0.27**	-0.05
Autumn	**+0.20**	**+0.31**	-0.20	**+0.31**
1956-2013				
Period	**NAO**	**AO**	**SCA**	**EA**
Annual	**+0.40**	+0.12	+0.08	+0.08
Winter	**+0.46**	**+0.50**	+0.10	**+0.35**
Spring	**+0.28**	**+0.36**	+0.02	-0.02
Summer	**+0.31**	-0.01	-0.17	**+0.30**
Autumn	**+0.36**	+0.18	-0.11	**+0.30**
1997-2015				
Period	**NAO**	**AO**	**SCA**	**EA**
Annual	+0.31	+0.31	0.00	+0.15
Winter	**+0.62**	**+0.67**	-0.19	+0.40
Spring	+0.22	**+0.53**	-0.05	-0.05
Summer	+0.20	-0.01	**-0.48**	+0.21
Autumn	-0.07	-0.04	-0.31	+0.18

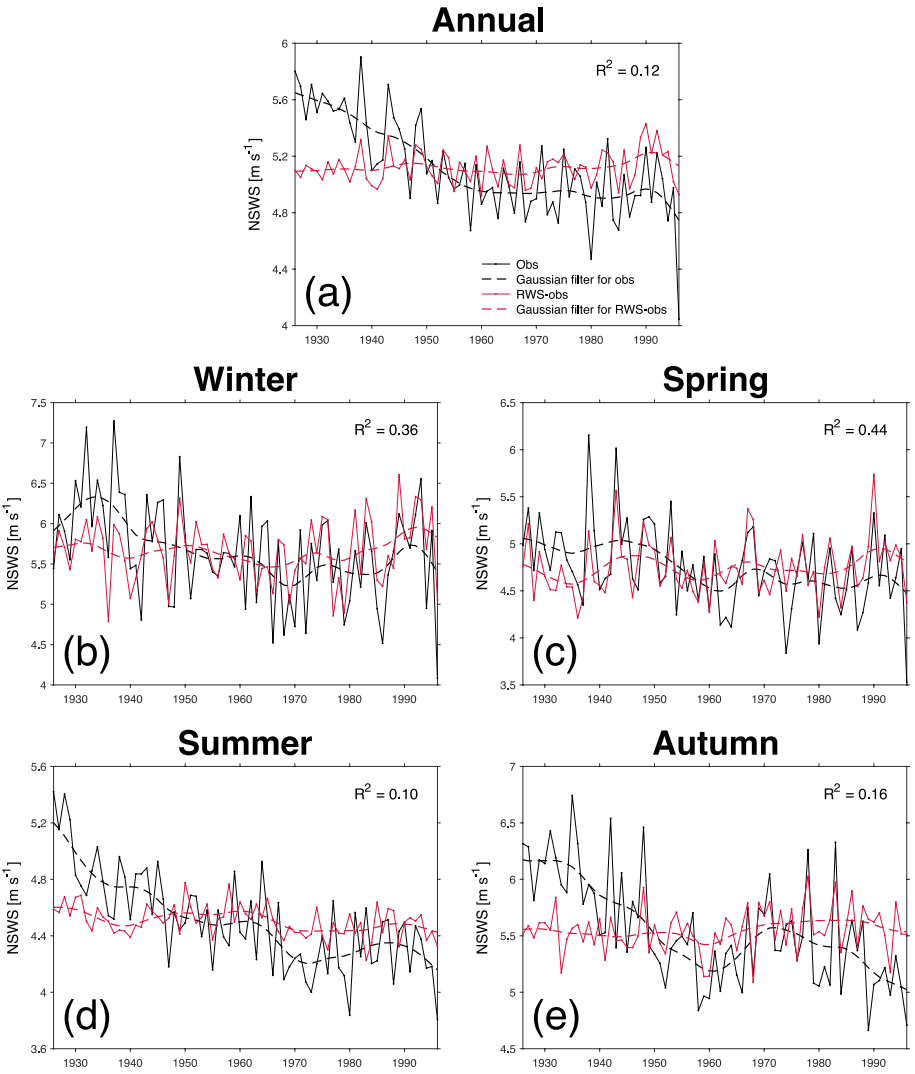

Fig. 5 Comparison between mean (i.e., average over all stations across Sweden) annual series of observed NSWS (black line) and RWS-obs (red line) for 1926–1996. The low-frequency variability is shown with the dashed lines of the applied Gaussian-weighted average (15-year windows)

4.3 Correlation with atmospheric circulation modes

The relationship between observed NSWS and the 4 different indexes of atmospheric circulation is investigated by calculating the Pearson's correlation for 1926–1996 annual and seasonal series (Table 3). NAO displays a significant ($p < 0.05$) positive correlation annually and for all the seasons, except for summer. When plotting the NAO index versus the observed NSWS (Fig. S2 in the supplementary material), it is evident that NAO well follows the low-frequency variability of observed wind (especially for winter, when r is

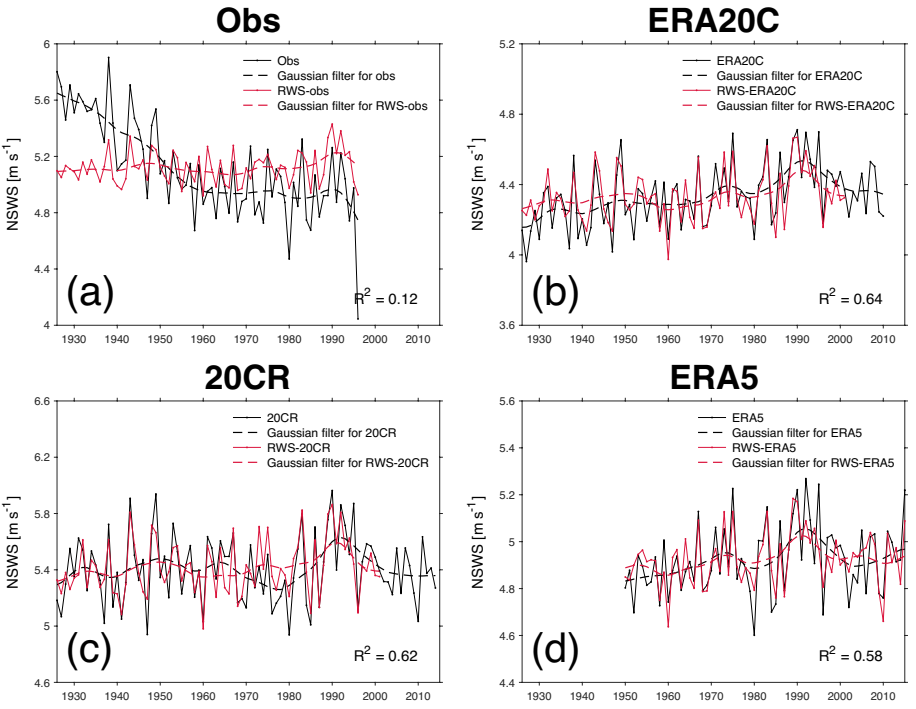

Fig. 6 NSWS *vs.* RWS. **a** Comparison between mean (i.e., average over all stations) annual series of observed NSWS (black line) and RWS-obs (red line). **b** Comparison between mean (i.e., average over all nearby grid points) annual series of ERA20C NSWS (black line) and RWS-ERA20C (red line). **c** Comparison between mean (i.e., average over all nearby grid points) annual series of NSWS from 20CR (black line) and RWS-20CR (red line). **d** Comparison between mean (i.e., average over all nearby grid points) annual series of NSWS from ERA5 (black line) and RWS-ERA5 (red line). The low-frequency variability is shown with the dashed lines of the applied Gaussian-weighted average (15-year windows)

0.50, $p < 0.05$), but it does not match the periods of strong decreases, like the 1926–1960 slowdown. Similarly, the AO index correlates well with the wind speed variations for the annual, winter, spring, and autumn series, reaching correlation values of 0.53 ($p < 0.05$). The main reason for the mismatch between AO and wind speed series is that the periods of strong stilling in observed NSWS do not appear in the AO variations. Like NAO and AO, EA correlates well with the observed NSWS series for winter, spring, and autumn. SCA is the only circulation pattern that displays a significant ($p < 0.05$) negative correlation (−0.27) for summer, while for the other seasons and annually, r values are low and not significant. Table 3 further explores the correlation between the 4 indexes of atmospheric circulation modes and the observed NSWS anomaly series of Minola et al. (2016, 2021) for 1956–2013 and 1997–2015, respectively. The relationships found for 1926–1996 are confirmed by these other NSWS series. In fact, NAO, AO, and EA correlate well especially during winter for these datasets too, while SCA shows a strong negative correlation for summer (even if it is not significant for 1956–2013).

Overall, all the selected indexes of atmospheric circulation patterns correlate well, even for different seasons, with the observed NSWS variability across Sweden. This shows that

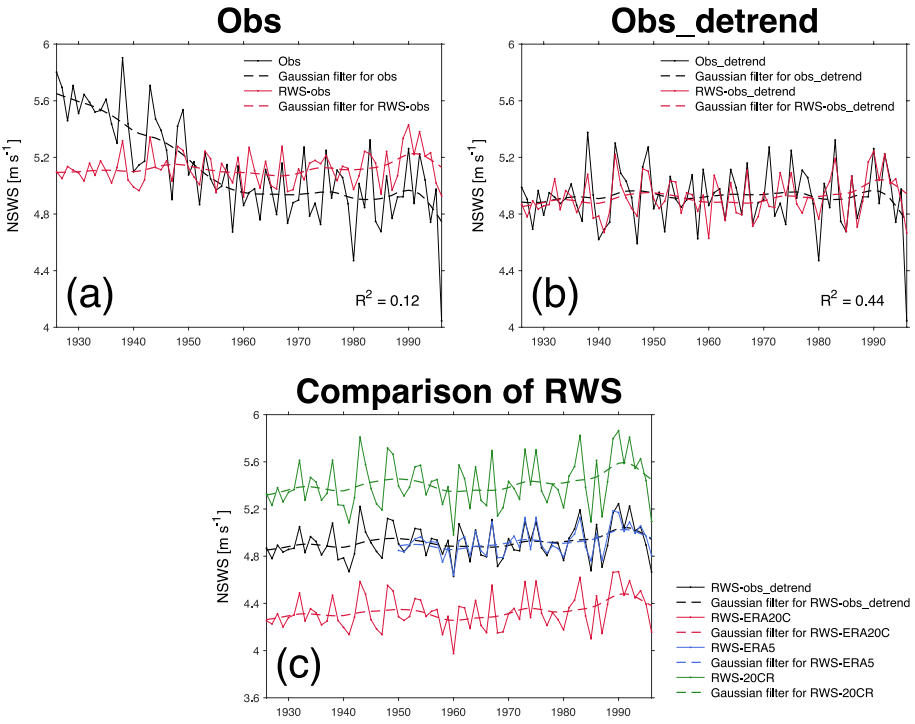

Fig. 7 RWS for NSWS observed *vs.* observed-detrended: **a** Comparison between mean (i.e., average over all stations) annual series of observed NSWS (black line) and RWS-obs (red line) for 1926–1996. **b** Comparison between mean (i.e., average over all stations) annual series of observed-detrended NSWS (black line) and RWS-obs_detrend (red line) for 1926–1996. **c** Comparison between RWS-obs_detrend (black line), RWS-ERA20C (red line), RWS-ERA5 (blue line), and RWS-20CR (green line). The low-frequency variability is shown with the dashed lines of the applied Gaussian-weighted average (15-year windows)

large-scale atmospheric circulation may play a crucial role in explaining the changes and variations of observed wind, especially when it comes to its low-frequency variability.

4.4 Reconstructing NSWS variability

Given the strong influence of large-scale atmospheric circulation on NSWS variability (see Sect. 4.3), we use all 4 indexes of atmospheric circulation modes (i.e., NAO, AO, SCA, and EA) to reconstruct observed NSWS using the MLR. The reconstructed observed NSWS (hereafter, RWS-obs) is calculated using all 4 indexes as the combination of both NAO, AO, SCA, and EA can explain a higher variance (R^2) of the observed NSWS compared to the use of just one index or a combination of two or three of them (e.g., R^2 up to 0.44 for spring). Figure 5 compares the mean annual and seasonal series of observed NSWS and RWS-obs for 1926–1996. Annually, the RWS-obs captures the interannual variability and the small interdecadal fluctuations (e.g., variability with a period of change of around 5 years, as during 1980–1990) of the observed NSWS series. But RWS-obs does not display the clear slowdown for 1926–1960, which therefore cannot be explained by the large-scale atmospheric circulation changes. Seasonally, a similar pattern can be noticed:

RWS-obs series follow the cyclical changes of observed NSWS, but do not simulate periods of evident decreasing trend, such as the 1926–1960 slowdown. For example, for autumn, the second period with a marked slowdown starts earlier than for the other seasons (1985 rather than 1990; see Fig. 3); when looking at the period 1926–1996, it is already possible to identify 11 years (1985–1996) of such slowdown, which goes until 2003. The RWS-obs for autumn does not show both the significant 1926–1960 slowdown and the evident 11-year decrease of NSWS during 1985–1996. Similarly, when reconstructing the NSWS for 1956–2013 (from the dataset of Minola et al. 2016; see Fig. S3 in the supplementary material), all the RWS-obs series calculated using the 4 indexes of teleconnection patterns do not capture the evident 1990–2003 slowdown both annually and seasonally, similar to what was already seen for autumn during 1985–1996.

Recalling what is seen in Sect. 4.2, ERA20C, 20CR, and ERA5 cannot reproduce as well the evident observed decrease during 1926–1960 and 1990–2003. But all these reanalyses go along with the observed low-frequency variability. This resembles the behavior of the RWS-obs calculated using the teleconnection-pattern indexes, which also does not simulate the periods of significant decrease. Therefore, we also reconstruct the NSWS of ERA20C (hereafter, RWS-ERA20C), ERA5 (hereafter, RWS-ERA5), and 20CR (RWS-20CR). Those RWS series well reproduce the variability of NSWS in ERA20C ($R^2 = 0.64$), 20CR ($R^2 = 0.62$), and ERA5 ($R^2 = 0.58$) (Fig. 6). Instead, RWS-obs can only explain 0.12 of the variance of observed NSWS (mostly because RWS-obs does not capture the 1926–1960 slowdown, not-driven by large-scale atmospheric circulation changes). This confirms that all the selected reanalyses can simulate NSWS variations driven by large-scale atmospheric circulation, but cannot include the 1926–1960 and 1990–2003 periods of marked stilling, which may not be caused by changes in large-scale atmospheric circulation patterns.

To further confirm that the strong 1926–1960 decreasing trend is not driven by large-scale atmospheric circulation changes, the mean observed NSWS series has been detrended (hereafter, obs_detrend), which means that the 1926–1960 negative trend has been removed from the mean series. The reconstructed NSWS series for obs_detrend (hereafter, RWS-obs_detrend) well follows the variability of the NSWS obs_detrend series, with a R^2 of 0.44, much greater than the R^2 of 0.12 for RWS-obs (Fig. 7). RWS-obs_detrend agrees as well with RWS-ERA20, RWS-ERA5, and RWS-20CR. This further confirms that the low-frequency fluctuations in NSWS driven by the large-scale atmospheric circulation variability are captured by all the reanalyses. But the strong decreasing trends (e.g., -0.24 m s^{-1} dec^{-1} for 1926–1960, significant at $p < 0.05$), which were observed both during 1926–1960 and 1990–2003 and not simulated by the reanalysis products, should not be driven by changes in the large-scale atmospheric circulation.

5 Summary and discussion

This study investigates the variability and changes of observed NSWS across Sweden since 1926, covering a centennial-scale time period. Even if previous studies have explored wind changes across Sweden, it is the first time that observed wind speed series are investigated for such an unprecedented length of time, which allows the comparison of various decadal-scale fluctuations of NSWS. By combining the 1926–1996 wind series here with the 1956–2013 dataset of Minola et al. (2016) and the 1997–2019 one of Minola et al. (2021), it was shown that NSWS underwent various phases of change during 1926–2019: (a) a clear slowdown during 1926–1960;

(b) a stabilization from 1960 to 1990; (c) another clear slowdown during 1990–2003; (d) a slight recovery/stabilization period for 2003–2014, which may continue with a possible new slowdown. When comparing the wind variability with the one of different indexes of atmospheric circulation patterns (i.e., NAO, AO, SCA, and EA), only the low-frequency variability of observed NSWS correlates well with the large-scale circulation variations: large-scale atmospheric circulation changes cannot explain the strong stilling during 1926–1960 and 1990–2003. Instead, they can explain small fluctuations, as different phases of changes in NSWS observed after 2003. In a similar way, also the reanalysis products (i.e., ERA20C, 20CR, and ERA5) do not simulate the robust decreasing trends during 1926–1960 and 1990–2003, but, instead, can only reproduce low-frequency variations. In fact, the 1926–1996 reconstructed NSWS, calculated by multiple regression using the different indexes of atmospheric circulation patterns, can explain only 0.12 of the observed wind variability. But when the strong decreasing trend during 1926–1960 is removed, the explained variability of the reconstructed wind increases to 0.44: large-scale atmospheric circulation changes are the most likely main drivers for the relative-small fluctuations of NSWS occurring over the past 100 years, but they cannot explain the significant decreasing trends of wind speed.

This study highlights that the 1926–1960 and 1990–2003 periods of evident slowdown drive most of the stilling in the last century. Those negative trends appear in every season, showing that the reason behind such stilling is not something occurring seasonally. In addition, the robust trends of those periods are not found in the reanalysis products: as reanalyses have proven to be able to properly simulate large-scale atmospheric circulation variations (Poli et al. 2016), such evident decreasing trends cannot be fully attributed to changes in atmospheric circulation patterns (Torralba et al. 2017). Instead, large-scale atmospheric changes can only explain the low-frequency variations of NSWS. In particular, no single index of atmospheric circulation pattern can fully reconstruct the relative-small variations in NSWS. Each index may be able to better explain the NSWS variability to some extent at a specific season (e.g., strong NAO influence during winter; Minola et al. 2016). But the indexes all together generate a higher amount of explanatory power in the reconstructed wind series (Zeng et al. 2019). This is because different teleconnections may interact with each other (e.g., EA modulates the location and the strength of the NAO dipole; Moore et al. 2011), and are complementary indicators in explaining climate changes and variations (Vicente-Serrano et al. 2016). Therefore, the low-frequency variability of NSWS cannot be simply linked to just a single atmospheric circulation pattern, but it should rather be resolved by the combined effects of variations in various teleconnection patterns (Shen et al. 2021a).

Shen et al. (2021a) found that centennial-scale changes of NSWS over China are mainly driven by the combined effects of large-scale ocean–atmosphere circulations. Instead, across Sweden, large-scale atmospheric circulation changes can only explain the low-frequency variations of NSWS, with the internal variability not being the reason behind the clear slowdown during 1926–1960 and 1990–2003. At the centennial scale, variations in large-scale atmospheric circulation patterns seem to drive cyclical decadal changes in NSWS, while the contribution of other factors (i.e., changes in surface friction) to the stilling across Sweden seems to be considerable (as it may explain the periods of evident decreasing trends). This is in line with what was found by model simulations at a global scale, where internal variability acted mainly to increase the NSWS from 1968 to 2014 through cyclical phases of change, while the contributions of other factors to the global terrestrial stilling after the 1960s were considerable (Shen et al. 2021b). Among the possible

factors which could have affected past wind changes across Sweden, Minola et al. (2021) have already investigated the contribution of changes in forest cover to the observed wind variability during 1997–2019. Unfortunately, this study cannot attribute the observed stilling to such factors. For example, the lack of orthophotos at a centennial scale does not allow quantifying the contribution of forest cover changes to the observed trend for the time period considered in this study. Other factors which can be included among the possible factors at the origin of the evident periods of stilling are land-use change driven by urbanization (Chen et al. 2020), anthropogenic aerosol emissions (Li et al. 2016), and aging of measuring instruments (Azorin-Molina et al. 2018b).

This study has also shown that current reanalysis products are not able to properly reproduce the actual changes and variations in observed NSWS. In fact, wind series obtained from reanalysis datasets only display decadal low-frequency variations, but do not reproduce the evident slowdown during 1926–1960 and 1990–2003. This is in line with what is shown by Torralba et al. (2017) and Minola et al. (2021), which evidenced the inability of reanalysis datasets in reproducing the observed decline of surface winds as they do not include some drivers of wind speed variability such as changes in surface roughness. To overcome the lack of global coverage and long historical records of wind observations, researchers have largely relied upon reanalysis data for wind resource assessment to estimate revenues of electricity production from wind farms (Pryor et al. 2009; Holt and Wang 2012). Therefore, it is necessary to careful weight their conclusions as those analyses based on reanalysis products may have overestimated wind statistics as the wind series they have used may not reflect actual changes in surface winds (i.e., they do not include the past observed stilling).

To conclude, as already revealed by Minola et al. (2021), the variability of observed NSWS across Sweden is driven by both changes in large-scale atmospheric circulation and other factors such as modification in surface roughness, which interplay in causing the observed wind variations. This study adds that low-frequency variability can be attributed mainly to variations in atmospheric patterns, which cannot explain the periods of evident stilling: these strong slowdown trends that drive most of the stilling in the last century should be driven by other factors including land-use and cover change and/or anthropogenic aerosol emissions. Future studies should focus on the quantification of the contribution of these factors.

Supplementary Information The online version contains supplementary material available at https://doi.org/10.1007/s10584-023-03525-0.

Author contribution Conceptualization: Lorenzo Minola, Cesar Azorin-Molina, Erik Engström, Deliang Chen; data curation: Lorenzo Minola, Jessika Lönn, Chunlüe Zhou, Erik Engström, Lennat Wern, Sverker Hellström; methodology: Lorenzo Minola, Jessika Lönn, Cesar Azorin-Molina, Cheng Shen; formal analysis and investigation: Lorenzo Minola, Jessika Lönn; writing - original draft preparation: Lorenzo Minola; writing - review and editing: Lorenzo Minola, Jessika Lönn, Cesar Azorin-Molina, Chunlüe Zhou, Erik Engström, Lennat Wern, Sverker Hellström, Gangfeng Zhang, Cheng Shen, Alessandro Pezzoli, Deliang Chen; funding acquisition: Cesar Azorin-Molina, Erik Engström, Deliang Chen.

Funding Open access funding provided by University of Gothenburg. This study was funded by Swedish FORMAS (2019–00509, 2019-01520) and VR (2017–03780, 2019–03954), as well as the Swedish National Strategical Research Programs BECC and MERGE. Lorenzo Minola is founded by the International Postdoc grant from the Swedish Research Council (2021–00444).

Data availability The 1926–1996 observed NSWS data which has been used in this study is openly available at the following link: http://rcg.gvc.gu.se/LM1/.

Declarations

Competing interests The authors declare no competing interests.

Open Access This article is licensed under a Creative Commons Attribution 4.0 International License, which permits use, sharing, adaptation, distribution and reproduction in any medium or format, as long as you give appropriate credit to the original author(s) and the source, provide a link to the Creative Commons licence, and indicate if changes were made. The images or other third party material in this article are included in the article's Creative Commons licence, unless indicated otherwise in a credit line to the material. If material is not included in the article's Creative Commons licence and your intended use is not permitted by statutory regulation or exceeds the permitted use, you will need to obtain permission directly from the copyright holder. To view a copy of this licence, visit http://creativecommons.org/licenses/by/4.0/.

References

Abhishek A, Lee J-Y, Keener TC, Jeffery Yang Y (2010) Long-term wind speed variations for three Midwestern U.S. cities. J Air Waste Manag Assoc 60:1057–1064. https://doi.org/10.3155/1047-3289.60.9.1057

Azorin-Molina C, Vicente-Serrano SM, McVicar TR et al (2014) Homogenization and assessment of observed near-surface wind speed trends over Spain and Portugal, 1961–2011. J Clim 27:3692–3712. https://doi.org/10.1175/JCLI-D-13-00652.1

Azorin-Molina C, Rehman S, Guijarro JA, McVicar TR, Minola L, Chen D, Vicente-Serrano SM (2018a) Recent trends in wind speed across Saudi Arabia, 1978–2013: a break in the stilling. Int J Climatol 38:e966–e984. https://doi.org/10.1002/joc.5423

Azorin-Molina C, Asin J, McVicar TR, Minola L, Lopez-Moreno JI, Vicente-Serrano SM, Chen D (2018b) Evaluating anemometer drift: a statistical approach to correct biases in wind speed measurements. Atmos Res 203:175–188. https://doi.org/10.1016/j.atmosres.2017.12.010

Berard J (2021) Ny statistic över installerad vindkraft 2020. Energimyndigheten. https://www.energimyndigheten.se/nyhetsarkiv/2021/ny-statistik-over-installerad-vindkraft-2020/. Accessed 9 Mar 2023

Bett PE, Thornton HE, Clark RT (2017) Using the twentieth century reanalysis to assess climate variability for the European wind industry. Theor Appl Climatol 127:61–80. https://doi.org/10.1007/s00704-015-1591-y

Bing D, Zhaoyin Y, Wupeng D, Xiaoyi F, Yonghong L, Chen C, Yan L (2021) Cooling the city with "natural wind": construction strategy of urban ventilation corridors in China. IOP Conf Ser: Earth Environ Sci 657:012009. https://doi.org/10.1088/1755-1315/657/1/012009

Blackburn M, Hoskins BJ (2001) The UK record-breaking wet autumn 2000. Universities Global Atmospheric Modelling Programme Newsletter. http://www.met.rdg.ac.uk/~mike/autumn2000/son00_article_fm.pdf. Accessed 9 Mar 2023

Chen X, Jeong S, Park H, Kim J, Park C-R (2020) Urbanization has strong impacts than regional climate change on wind stilling: a lesson from South Korea. Earth Environ Sci 15:054016. https://doi.org/10.1088/1748-9326/ab7e51

Comas-Bru L, Hernández A (2018) Reconciling North Atlantic climate modes: revised monthly indices for the East Atlantic and the Scandinavian patterns beyond the 20th century. Earth Syst Sci Data 10:2329–2344. https://doi.org/10.5194/essd-10-2329-2018

Compo GP, Whitaker JS, Sardeshmukh PD et al (2011) The Twentieth Century Reanalysis project. Quart J Roy Meteor Soc 137:1–28. https://doi.org/10.1002/qj.776

Dee DP, Uppala SM, Simmons AJ et al (2011) The ERA-Interim reanalysis: configuration and performance of the data assimilation system. Quart J Roy Meteor Soc 137:553–597. https://doi.org/10.1002/qj.828

Engström E, Azorin-Molina C, Wern L, Hellström S, Zhou C, Chen D (2022) Data rescue of historical wind observations in Sweden since the 1920s. Earth Syst Sci Data. Preprint. https://doi.org/10.5194/essd-2023-2

Gibbons JD, Chakraborti S (2003) Nonparametric statistical inferences. Marcel Dekker Inc., New York

Gilbert RO (1987) Statistical method for environmental pollution monitoring. Van Nostrand Reinhold Co., New York

Grundström M, Hak C, Chen D, Hallquist M, Pleijel H (2015) Variation and co-variation of PM_{10}, particle number concentration, NO_x and NO_2 in the urban air – relationship with wind speed, vertical temperature gradient and weather type. Atmos Environ 120:317–327. https://doi.org/10.1016/j.atmosenv.2015.08.057

Hamed KH, RamachandraRao A (1998) A modified Mann-Kendall trend test for autocorrelated data. J Hydrol 204:182–196. https://doi.org/10.1016/S0022-1694(97)00125-X

Hersbach H, Bell B, Berrisford P et al (2020) The ERA5 global reanalysis. Quart J Roy Meteor Soc 146:1999–2049. https://doi.org/10.1002/qj.3803

Holt E, Wang J (2012) Trends in wind speed at wind turbine height of 80 m over the contiguous United States using the North American Regional Reanalysis (NARR). J Appl Meteorol Climatol 51:2188–2202. https://doi.org/10.1175/JAMC-D-11-0205.1

Hurrel JW, Kushnir Y, Ottersen G, Visbeck M (2003) An overview of the North Atlantic Oscillation. In: Hurrel JW et al (ed) The North Atlantic Oscillation: climate significance and environmental impact, Geophys Monogr Ser, pp 1–35

IPCC (2013) Climate change 2013: the physical science basis. Cambridge University Press, Cambridge.https://doi.org/10.1017/CBO9781107415324

IPCC (2014) Climate change 2014: mitigation of climate change. Cambridge University Press, Cambridge.https://doi.org/10.1017/CBO9781107415416

IPCC (2021) Climate change 2021: the physical science basis. Cambridge University Press, Cambridge.https://doi.org/10.1017/9781009157896

Kim JC, Paik K (2015) Recent recovery of surface wind speed after decadal decrease: a focus on South Korea. Clim Dyn 45:1699–1712. https://doi.org/10.1007/s00382-015-2546-9

Laapas M, Venäläinen A (2017) Homogenization and trend analysis of monthly mean and maximum wind speed time series in Finland, 1959–2015. Int J Climatol 37:4803–4813. https://doi.org/10.1002/joc.5124

Li Z, Lau WK-M, Ramanathan V et al (2016) Aerosol and monsoon climate interactions over Asia. Rev Geophys 54:8666–8929. https://doi.org/10.1002/2015RG000500

Lin C, Yang K, Qin J, Fu R (2013) Observed coherent trends of surface and upper-air wind speed over China since 1960. J Clim 26:2891–2903. https://doi.org/10.1175/JCLI-D-12-00093.1

McVicar TR, Roderick ML, Donohue RJ et al (2012) Global review and synthesis of trends in observed terrestrial near-surface wind speeds: implications for evaporation. J Hydrol 416–417:182–205. https://doi.org/10.1016/j.jhydrol.2011.10.024

Minola L, Azorin-Molina C, Chen D (2016) Homogenization and assessment of observed near-surface wind speed trends across Sweden, 1956–2013. J Clim 29:7397–7415. https://doi.org/10.1175/JCLI-D-15-0636.1

Minola L, Zhang F, Azorin-Molina C, SafaeiPirooz AA, Flay RGJ, Chen D (2020) Near-surface mean and gust wind speeds in ERA5 across Sweden: towards an improved gust parametrization. Clim Dyn 55:887–907. https://doi.org/10.1007/s00382-020-05302-6

Minola L, Reese H, Lai H-W, Azorin-Molina C, Guijarro JA, Son S-W, Chen D (2021) Wind stilling-reversal across Sweden: the impact of land-use and large-scale atmospheric circulation changes. Int J Climatol 42:1049–1071. https://doi.org/10.1002/joc.7289

Moore GWK, Pickart RS, Renfrew IA (2011) Complexities in the climate of the subpolar North Atlantic: a case study from the winter of 2007. Quart J Roy Meteor Soc 137:757–767. https://doi.org/10.1002/qj.778

Pedroni P (1999) Critical values for cointegration tests in heterogeneous panels with multiple regressors. Oxf Bull Econ Stat 61:653–670. https://doi.org/10.1111/1468-0084.0610s1653

Poli P, Hersbach H, Dee DP et al (2016) ERA-20C: an atmospheric reanalysis of the twentieth century. J Clim 29:4083–4097. https://doi.org/10.1175/JCLI-D-15-0556.1

Pryor SC, Barthelmie RJ, Young DT et al (2009) Wind speed trends over the contiguous United States. J Geophys Res Atmos 114:D14105. https://doi.org/10.1029/2008JD011416

Ramon J, Lledó L, Torralba V, Soret A, Doblas-Reyes FJ (2019) What global reanalysis best represents near-surface winds? Quart J Roy Meteor Soc 145:3236–3251. https://doi.org/10.1002/qj.3616

Rayner DP (2007) Wind run changes: the dominant factor affecting pan evaporation trends in Australia. J Clim 20:3379–3394. https://doi.org/10.1175/JCLI4181.1

Roderick ML, Rotstayn LD, Farquhar GD, Hobbins MT (2007) On the attribution of changing pan evaporation. Geophys Res Lett 34:L17403. https://doi.org/10.1029/2007GL031166

Scott E (2021) Changes in ocean circulation patterns. In: Scott E (ed) Threats to the Arctic, Elsevier Inc., pp 27–44

Shen C, Zha J, Wu J, Zhao D (2021a) Centennial-scale variability of terrestrial near-surface wind speed over China from reanalysis. J Clim 34:5829–5846. https://doi.org/10.1175/JCLI-D-20-0436.1

Shen C, Zha J, Zhao D, Wu J, Fan W, Yang M, Li Z (2021b) Estimating centennial-scale changes in global terrestrial near-surface wind speed based on CMIP6 GCMs. Environ Res Lett 16:084039. https://doi.org/10.1088/1748-9326/ac1378

Shi P, Zhang G, Kong F, Chen D, Azorin-Molina C, Guijarro JA (2019) Variability of winter haze over the Beijing-Tianjin-Hebei region tied to wind speed in the lower troposphere and particulate sources. Atmos Res 215:1–11. https://doi.org/10.1016/j.atmosres.2018.08.013

Torralba V, Doblas-Reyes FJ, Gonzalez-Reviriego N (2017) Uncertainty in recent near-surface wind speed trends: a global reanalysis intercomparison. Environ Res Lett 12:114019. https://doi.org/10.1088/1748-9326/aa8a58

Vautard R, Cattiaux J, Yiou P, Thépaut J-N, Ciais P (2010) Northern hemisphere atmospheric stilling partly attributed to an increase in surface roughness. Nature Geosci 3:456–761. https://doi.org/10.1038/ngeo979

Vicente-Serrano SM, Garciá R, Barriopedro D et al (2016) The Westerly Index as complementary indicator of the North Atlantic oscillation in explaining drought variability across Europe. Clim Dyn 47:845–863. https://doi.org/10.1007/s00382-015-2875-8

Von Storch H, Zwiers FW (1999) Statistical analysis in climate research. Cambridge University Press, Cambridge

Wu J, Zha J, Zhao D, Yang Q (2018) Changes in terrestrial near-surface wind speed and their possible causes: an overview. Clim Dyn 51:2039–2078. https://doi.org/10.1007/s00382-017-3997-y

Yu J, Zhou T, Jiang Z, Zou L (2019) Evaluation of near-surface wind speed changes during 1979 to 2011 over China based on five reanalysis datasets. Atmos 10:804. https://doi.org/10.3390/atmos10120804

Zeng Z, Ziegler AD, Searchinger T et al (2019) A reversal in global terrestrial stilling and its implications for wind energy production. Nat Clim Chang 9:979–985. https://doi.org/10.1038/s41558-019-0622-6

Zeng Z, Piao S, Li LZX et al (2018) Global terrestrial stilling: does Earth's greening play a role? Environ Res Lett 13:124013. https://doi.org/10.1088/1748-9326/aaea84

Zhang Z, Wang K (2020) Stilling and recovery of the surface wind speed based on observation, reanalysis, and geostrophic wind theory over China from 1960 to 2017. J Clim 33:3989–4008. https://doi.org/10.1175/JCLI-D-19-0281.1

Zhang G, Azorin-Molina C, Shi P, Lin D, Guijarro JA, Kong F, Chen D (2019) Impact of near-surface wind speed variability on wind erosion in the eastern agro-pastoral transitional zone of Northern China, 1982–2016. Agric for Meteorol 271:102–115. https://doi.org/10.1016/j.agrformet.2019.02.039

Zheng CW, Pan J, Lin CY (2016) Global oceanic wind speed trends. Ocean Coast Manag 129:15–24. https://doi.org/10.1016/j.ocecoaman.2016.05.001

Zhou C, Azorin-Molina C, Engström E, Minola L, Wern L, Hellström S, Lönn J, Chen D (2022) HomogWS-se: a century-long homogenized dataset of near-surface wind speed observations since 1925 rescued in Sweden. Earth Syst Sci Data 14:2167–2177. https://doi.org/10.5194/essd-14-2167-2022

Publisher's note Springer Nature remains neutral with regard to jurisdictional claims in published maps and institutional affiliations.

Authors and Affiliations

Lorenzo Minola[1,2,3] · Jessika Lönn[1] · Cesar Azorin-Molina[3] · Chunlüe Zhou[1] · Erik Engström[4] · Lennart Wern[4] · Sverker Hellström[4] · Gangfeng Zhang[5,6] · Cheng Shen[1] · Alessandro Pezzoli[2] · Deliang Chen[1]

[1] Department of Earth Sciences, University of Gothenburg, Gothenburg, Sweden

[2] Interuniversity Department of Regional and Urban Studies and Planning (DIST), Politecnico and University of Turin, Turin, Italy

[3] Climate, Atmosphere and Ocean Laboratory (Climatoc-Lab), Centro de Investigaciones Sobre Desertificación, Consejo Superior de Investigaciones Científicas (CIDE, CSIC-UV-Generalitat Valenciana), Moncada, Valencia, Spain

[4] Swedish Meteorological and Hydrological Institute (SMHI), Norrköping, Sweden

[5] State Key Laboratory of Earth Surface Processes and Resource Ecology, Beijing Normal University, Beijing, China

[6] Academy of Disaster Reduction and Emergency Management, Ministry of Emergency Management and Ministry of Education, Beijing Normal University, Beijing, China